

Article

Outdoor Thermal Comfort: Coupling Microclimatic Parameters with Subjective Thermal Assessment to Design Urban Performative Spaces

Mohamed H. Elnabawi ^{1,2,*}  and Neveen Hamza ³

¹ College of Engineering, Applied Science University (ASU), Bahrain, In Partnership with London South Bank University, London SE1 0AA, UK

² Faculty of Engineering, October University for Modern Sciences and Arts (MSA), Cairo 12566, Egypt

³ School of Architecture, Planning and Landscape, Newcastle University, Newcastle upon Tyne NE1 7RU, UK; neveen.hamza@ncl.ac.uk

* Correspondence: melnabawi@aucegypt.edu

Received: 6 November 2020; Accepted: 7 December 2020; Published: 11 December 2020



Abstract: Thermal comfort plays a main role in encouraging people to use outdoor spaces, specifically in hot arid and humid climates. The reconciliation of climatic aspects during the urban design phase is limited in implementation, due to the need for multidisciplinary collaboration between desperate scientific fields of climatology, urban planning, and urban environmental modelling. This paper aims to create an integrated interface between the microclimate, outdoor thermal comfort, and design guidelines. The investigation combines subjective and objective approaches, including on-site field measurements, a structured questionnaire using the seven-point American Society of Heating, Refrigerating and Air-Conditioning Engineers (ASHRAE 55) thermal sensation votes, and a correlation study of these votes and the microclimatic parameters. Pedestrian thermal comfort was then examined under six shading scenarios, addressing the form and opening of shading devices using computational fluid dynamics. Modelling is based on four dependent variables: wind velocity, ventilation flow rate, air temperature, and the physiological equivalent temperature (PET) index. Findings indicate that the form and location of apertures of the shading devices were the dominant factors in achieving thermal comfort on the urban scale, and led to a reduction in air temperature and a physiological equivalent temperature of 2.3–2.4 °C. Subjective votes indicate that people who live in hot arid climates have a wider range of adaptation and tolerance to local climatic conditions. Accordingly, a psychometric chart, for the case study outdoor thermal comfort was developed.

Keywords: outdoor thermal comfort; physiological equivalent temperature (PET); thermal sensation votes (TSV); computational fluid dynamics (CFD)

1. Introduction

The 2020 Global Risks Perception survey issued by the World Economic Forum classified climate change and associated environmental matters as being in the top five global risks most likely to occur in the next decade. This is in addition to a report by the Intergovernmental Panel on Climate Change [1] and supported by public concerns, suggesting that global warming should be held at 1.5 °C to avoid significant damage to human wellbeing and the ecosystem. Climate change predictions suggest a high probability of a further rise in global temperatures by 1.5 °C between 2030 and 2052, if the present rate of increase remains unmanaged. In regions with hot arid climates, increases in air temperature may lead to increases in endangering life and mortality rates. Furthermore, human performance of mental and physical tasks diminishes at uncomfortably high temperatures, while illness and death caused by air pollution are likely to increase during extreme hot weather [2–4].

Even without the added thermal stress due to global warming, cities are at a higher risk than rural areas during hot weather and clear sky conditions, experiencing the phenomenon of elevated air temperatures than their surrounding urban environments—known as the urban heat island (UHI), [5–7]. UHI is attributed to rapid urbanisation and accelerated changes to outdoor surfaces [8,9]. Several studies have reported that by adapting certain urban configurations within the urban canopy layer (found in the air layer between the ground and the rooftops), improvements can be made to the local microclimate. This can enhance urban thermal comfort for inhabitants, particularly during the summer, such as by reducing heat-related illness [10–13]. Usually, urban thermal comfort design strategies tackle day-time conditions, when severe heat is most likely to occur during longer summer daylight hours [10]. An initial action to alleviate uncomfortable hot outdoor conditions in summer is to decrease or intercept the amount of radiation received on surfaces and people.

Since the ability to control the air temperature in urban spaces is limited, it is fairly simple to control exposure to direct sunlight by providing shade to improve urban occupants' thermal comfort [14,15]. Additionally, from a behavioural adjustment stance, seeking shade is considered the predominant adaptive behaviour taken by outdoor users on hot summer days [16]. However, the outdoor environment is heterogeneous and includes various types of urban forms, surface materials, and landscapes. These parameters combine to create a local microclimate by altering direct solar radiation and reflection patterns, wind speed, and direction.

Moreover, for a full assessment, subjective parameters, such as thermal perceptions and preferences, must also be examined and combined, since residents of hot countries tolerate higher temperatures than those in temperate ones [17–19]. Accordingly, thermal comfort indices or scales established in temperate areas are inapplicable elsewhere, providing the opportunity to use local subjective comfort data developed for the examined sites, and produce a better assessment of outdoor thermal comfort as related to locals using the space regularly [16,19–23].

However, the integration of subjective and objective parameters within the planning and design process is missing due to the poor interdisciplinary collaboration between climatologists, urban planners, and urban simulation experts [24–28]. Therefore, this study aims to facilitate such integration within the urban planning process into one framework, including microclimatic data and subjective thermal sensations in hot arid climates. The main objectives of this study are:

1. To evaluate pedestrians' thermal comfort perceptions and preferences in outdoor urban spaces in a hot arid climate;
2. To evaluate the cooling effect of different shading scenarios on air temperature, wind velocity, and subsequent improvement to outdoor thermal comfort;
3. To predict the performance of various shading scenarios on urban thermal comfort by triangulating the measured field data with the subjective outcomes from the social survey and the numerical modelling tools.

Study Context and Justifications

According to Gehl (2008), local sun and shade conditions may have a significant influence over people's desire to leave or stay in an outdoor space [29]. Pearlmutter et al. (2007) stated that shade is the predominant parameter steering the heat balance equation in an arid region [30]. Therefore, shading is considered key to improving urban thermal comfort in such a climate, mostly in summer [30–35]. Recently the efficacy of shading systems as a traditional climatic solution has been scrutinized [36–38]. Indeed, studies have reported a negative effect of shading systems with limited openings that restrict night purge, and surfaces take longer to cool, causing high air temperature and an increase in UHIs [38–41]. This indicates that the higher the sky view factor, the lower the UHI, especially at night [37]. In this respect, any shading proposals should be assessed, not only during the day when their positive effect is well known, but also at night when the positive effect might be reversed. Accordingly, to fulfil the paper's objectives, the study investigated an existing historical commercial alley in mid Cairo, Egypt. The location climate is classified as hot arid (BWh) based on the

Koppen-Geiger climate categorisation [42]. Al Khayamiya (Tentmakers) Alley has been preserved and represents a climate-conscious design acquired by trial and error of building experience (Figure 1).



Figure 1. Al Khayamiya Alley. Ancient town planners tried to avoid direct exposure to intense solar radiation.

The topology and form of the structure was designed and oriented to provide shade by screening solar radiation. The shading structure also has several different openings so that stratified air escapes at night, but daylight can penetrate the space to reduce the need for artificial lighting.

2. Methods

Urban thermal comfort is an interdisciplinary study, incorporating multi-disciplinary areas, such as meteorology, urban structure, psychology, and social behaviour. The local microclimate at the canyon level is of the utmost importance for thermal comfort assessment, yet, any urban thermal comfort assessment cannot only be based on objective parameters without including, subjective responses to the surrounding environment and urban configuration of the location. Accordingly, the proposed framework presented in Figure 2 is designed based on the interoperability of the different levels of assessment, and contextualises both the quantitative and qualitative characteristics of thermal sensations regarding a particular urban climate, including field measurements, structured questionnaires, and site observation as phase one, followed by computational fluid dynamics (CFD) parametric analysis as phase two, to overcome the lack of integrating the climatic analysis within the urban design stage, and to create an effective decision-making framework for urban planners and designers.

The objectives of the two phases are as follows:

1. Identify the major microclimate parameters for a hot arid climate;
2. Calculate the objective and subjective comfort index;
3. Calibrate the objective and subjective comfort index;
4. CFD parametric analysis based on objective and subjective parameters.

2.1. In Situ Field Measurements

In situ measurements were carried out for one week during the hot summer, and covered the five main microclimate parameters responsible for outdoor thermal comfort, based on ASHRAE Standard [43], of air temperature, wind velocity, relative humidity, and solar radiation, in addition to globe temperature. These field measurements were taken simultaneously with the pedestrians' subjective thermal perceptions survey, as described in the following section. Based on the preliminary data collected from the weather files for the last 30 years, the experimental data were collected between 26 June and 2 July 2012, as representative of a week in the hot summer season [44].

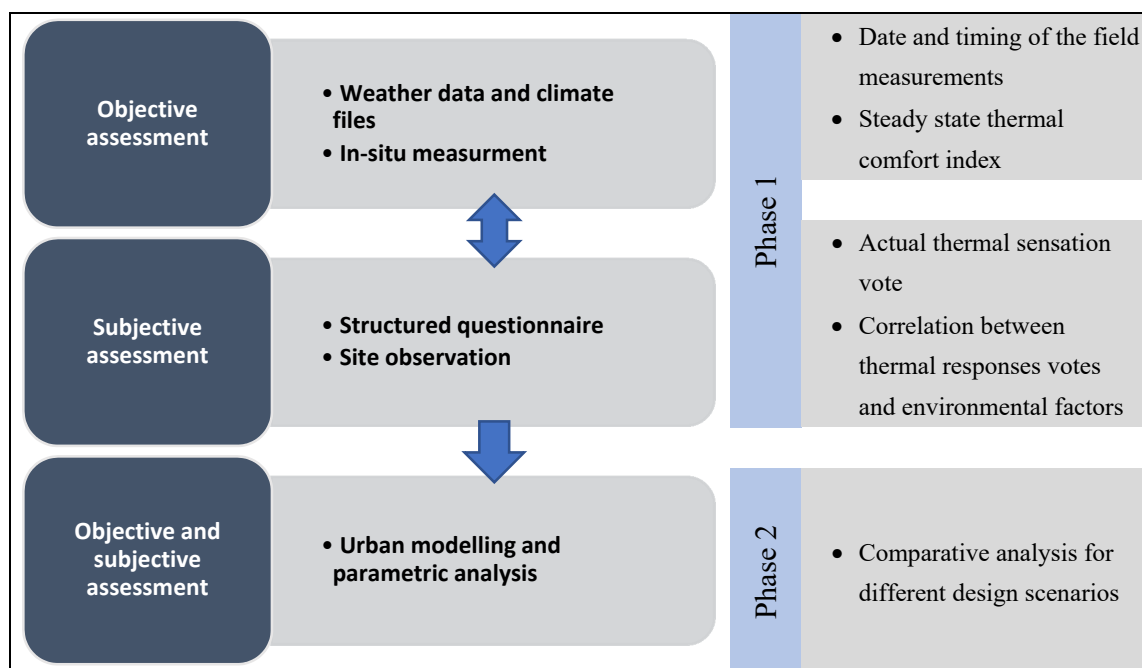


Figure 2. Methodological framework.

2.2. Questionnaire Survey

A structured survey took place concurrently with the in situ field measurements, with the main objective of rating the pedestrians' thermal perception. The structured questionnaire was based on the ASHRAE 7 point thermal sensation vote (TSV) scale (e.g., cold 3; cool 2; slightly cool 1; neutral 0; slightly warm 1; warm 2; and hot 3), in addition to a three point scale where the interviewees could identify their level of preference for wind and sun, such as "I want the wind/daylight to be weaker", "no change", and "I want the wind/daylight to be stronger". At the same time, observations were made of clothing units and metabolic rate, and estimates were recorded based on ASHRAE standards 55–2009 [45]. Accordingly, one hundred and sixty people were interviewed, of which 35% were women and 65% were men. The majority were between 25 and 34 years of age (35.8%), followed by the age group between 35 and 44 (24.2%), then the age group between 16 and 24 (19.2%), then 45–54 years old (11.7%), and over 55 (9.1%). Only participants who had direct and regular contact with the study area were interviewed.

2.3. CFD Modelling and Parametric Analysis

Following the field measurements and the questionnaire, parametric modelling was conducted using CFD, which is frequently used to assess urban microclimate based on the physiological equivalent temperature (PET) and acceptable comfort range obtained from the previous phase. CFD can resolve the transfer of heat and mass and their interaction with individual obstacles, such as buildings [46]. CFD can also be utilised for the analysis of the microclimate around individual buildings, which is classified as the building scale with typical distances of less than 100 m. Therefore, the CFD Fluent code 13.0 was used to examine the impact of six different shading scenarios, as shown in Figure 3, on the overall thermal comfort underneath, along with the existing or base case for validation purposes.

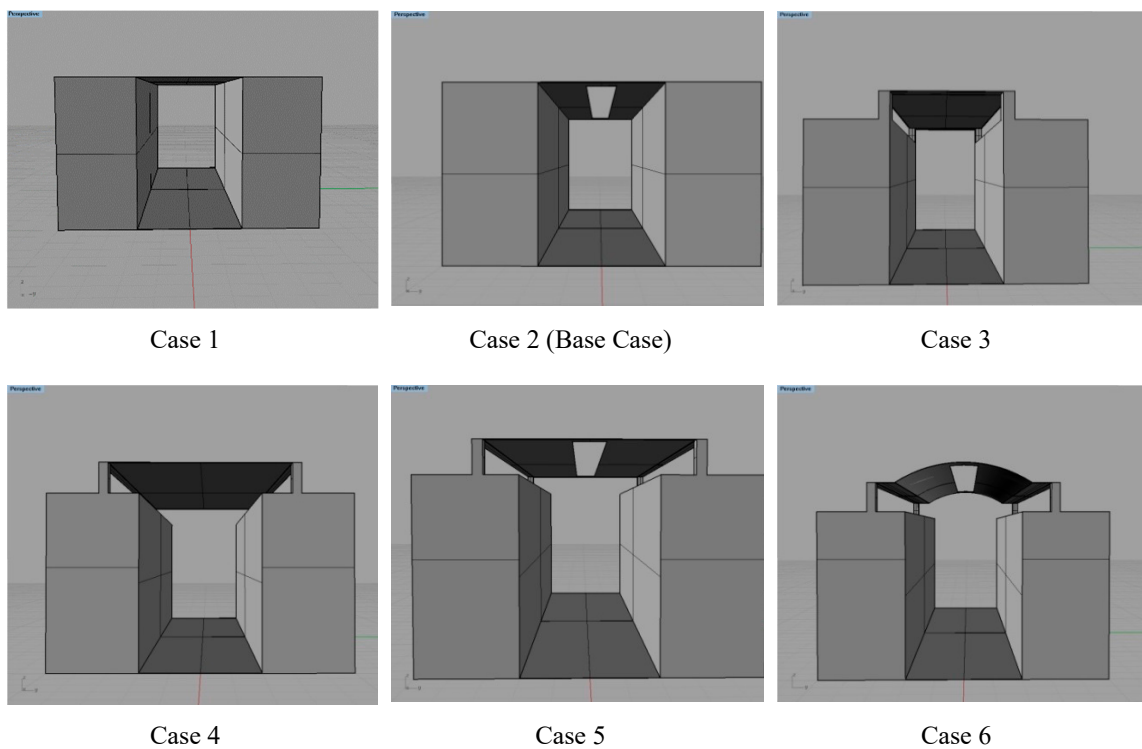


Figure 3. The examined case studies, including specific changes in the roof form and opening locations.

All scenarios had the same aspect ratio equal to 1.5, with the only difference between the cases being the roof's geometric form and the number and location of roof openings (Figure 3). The tested parameters were wind velocity, ventilation flow rate, and mean air temperature, which were used to analyse the impact of each case on the overall thermal comfort. The outcomes were compared with the PET comfort index reported from the site questionnaire. Parametric environment performance simulation analysis has proven to be a very efficient tool to assess different design proposals and their impact on human well-being [47].

2.3.1. CFD Simulation Model, Settings, and Atmospheric Boundary Layer ABL

To perform a reliable CFD simulation, the user has to deal with several uncertainties, starting with flow approximate equations, the level of detail in the geometric model, computational domain size, computational grid resolution and type, boundary conditions, discretisation schemes, initialisation data, and iterative convergence criteria. Any changes within these variables will completely affect the outcomes [48,49]. Therefore, a well-established framework or guidelines must be followed, the formation of which has been a major move regarding more reliable and accurate CFD simulations. For this reason, all of the simulations were regulated in accordance with the best practice guidelines (BPG) scenario for developing existing urban configurations [49], in which domain size, computational grid, boundary conditions, discretisation schemes, algorithms for pressure interpolation, and pressure-velocity coupling are all well prescribed, as stated in Table 1.

Table 1. Requisites for a consistent computational fluid dynamics (CFD) simulation [46,49,50] as applied on Figure 4.

Solution Method	Second Order Schemes or Above Should be Used to Solve Algebraic Equations
Residuals	In the range of 10^{-4} to 10^{-6} Multi-block structured mesh
Mesh	Carrying out sensitivity analysis with three levels of refinements where the ratio of cells for two consecutive grids should be at least 3.4
Turbulence model	Realisable k- ϵ turbulence model
Accuracy of studied buildings	Details of dimension equal to, or more than, 1 m to be included If H is the building height; lateral dimension = 2H + building width Flow direction dimension = 20H + building dimension in flow direction Vertical direction = 6H
Domain dimensions	While maintaining a blockage ratio below 3% (Franke et al., 2007; Tominaga et al., 2008b) Inflow: horizontally homogenous log law Atmospheric Boundary Layer (ABL) velocity profile—velocity inlet
Boundary conditions	Bottom: no-slip wall with standard wall functions Top and side: symmetry Outflow: pressure outlet

Apart from these common guidelines, there is a necessity to avoid any occurrence of the unintended streamwise gradients in the vertical profiles of the mean wind speed and turbulence quantities (horizontal inhomogeneity) as the flow travels from the inlet of the computational domain towards the modelled buildings. According to Blocken et al. [49], unplanned streamwise gradients can significantly affect the reliability of the modelling outcomes. In order to create an equilibrium atmospheric boundary layer (ABL), Richards and Hoxey [51] provided inlet profiles and wall boundary conditions that are consistent with the standard K-epsilon (k-e) model. Therefore, the inlet boundary condition was identified according to Equations (1)–(3), representing the velocity, turbulent kinetic energy, and turbulent dissipation rate, respectively, as recommended by Richards and Hoxey [51]:

$$U = \frac{u^*}{k} \ln\left(\frac{z + z_0}{z_0}\right) \quad (1)$$

$$K = \frac{u^{*2}}{\sqrt{C_u}} \quad (2)$$

$$\epsilon = \frac{u^{*3}}{k(z + z_0)} \quad (3)$$

(u^*) Friction velocity (m/s), (k) von Kármán constant (=0.40 or 0.42), (C_u) turbulence model constant, (z) height (m), and (z_0) aerodynamic roughness length (m), which is 0.5 m or 1.0 m depending on the wind direction.

While the ground boundary conditions were classified as rough and standard wall functions; Blocken et al. [52] derived the specific relationships between the roughness height (k_s) and roughness constant (C_s) (Equation (4) in order to have an accurate flow near the bottom surface.

$$k_s = \frac{9.793 z_0}{C_s} \quad (4)$$

The roughness length was assigned equal 2.0, representing city centres with a mixture of low- and high-rise building, according to Davenport roughness classification [53,54].

The settings of the applied boundary conditions were comprised of 3 m/s as inlet velocity approaching from the north direction and 35 °C as inlet air temperature, in addition to all other requirements presented in Table 1. The simulation was carried out using Ansys fluent code 13.0. The model employs the control volume technique and the Semi-Implicit Method for Pressure-Linked Equations (SIMPLE) velocity–pressure coupling algorithm with the second order upwind discretisation [49]. The turbulence kinetic energy (k) and its rate of dissipation (ϵ) are determined by Equations (5) and (6).

$$\frac{\partial}{\partial t}(\rho k) + \frac{\partial}{\partial x_j}(\rho k u_j) = \frac{\partial}{\partial x_j} \left[\left(\mu + \frac{\mu_t}{\sigma_k} \right) \frac{\partial k}{\partial x_j} \right] + G_k + G_b - \rho \epsilon - Y_M + S_k \quad (5)$$

$$\frac{\partial}{\partial t}(\rho \epsilon) + \frac{\partial}{\partial x_j}(\rho \epsilon u_j) = \frac{\partial}{\partial x_j} \left[\left(\mu + \frac{\mu_t}{\sigma_\epsilon} \right) \frac{\partial \epsilon}{\partial x_j} \right] + \rho C_1 S_\epsilon - \rho C_2 \frac{\epsilon^2}{k + \sqrt{\nu \epsilon}} + C_{1\epsilon} \frac{\epsilon}{k} C_{3\epsilon} G_b + S_\epsilon \quad (6)$$

(G_k) the generation of turbulent kinetic energy that arises due to mean velocity gradients, (G_b) generation of turbulent kinetic energy arising from buoyancy, (Y_M) the fluctuating dilation in compressible turbulence that contributes to the overall dissipation rate. (S_ϵ) and (S_k) source terms defined by the user. (α_k) and (α_ϵ) the turbulent Prandtl numbers for the turbulent kinetic energy and its dissipation.

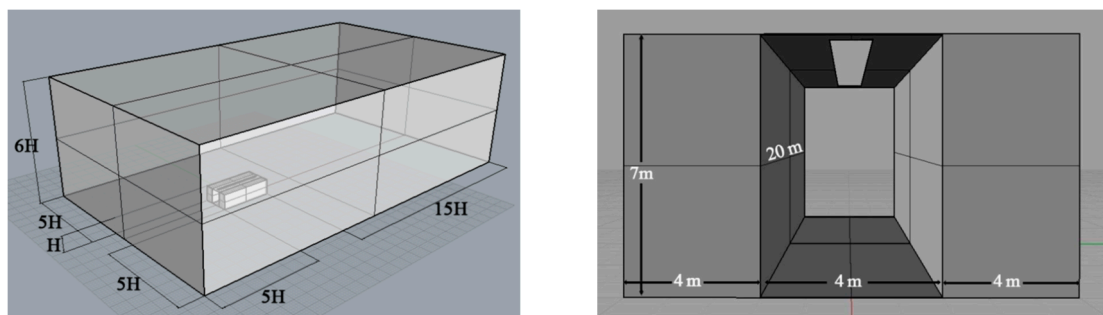


Figure 4. The model was placed in a computational domain with dimensions 147 m × 85 m × 45 m as X, Y, and Z (length, width, and height).

2.3.2. CFD Simulation Validation

Validation is essential to achieve accurate and reliable results for CFD studies on urban microclimate [55–57], which is the process of determining the degree to which a model is an accurate representation of the real world from the perspective of the intended uses of the model, as stated by the American Institute of Aeronautics and Astronautics [58]. According to several CFD best practice guidelines [56,59,60], on-site measurement validation represents the complex reality without simplification, and is therefore true validation data for numerical models [49]. Studies that fall into the sub-category of “real urban areas—with validation” include validation based on one or more of the simulation parameters with measurements. According to Toparlar et al. [46], for real urban areas, the field measurement of air temperature is relatively straightforward and has been widely used, especially in recent years. Therefore, the validation was typically performed by comparing the air temperature reported in the CFD with the stated values from the field data. The measurement point was in the middle of Al Khayamiya Alley. As shown in Figure 5, the model included all the important physical phenomena likely to occur, and these were gradually refined until a constant solution was achieved [61].

The mesh spacing was coarsened with 0.48 m as minimum spacing. Recommended skewness is below 0.98 as per the ANSYS FLUENT tutorial, and mesh spacing was refined for the areas around the model, to reach 0.24 m.

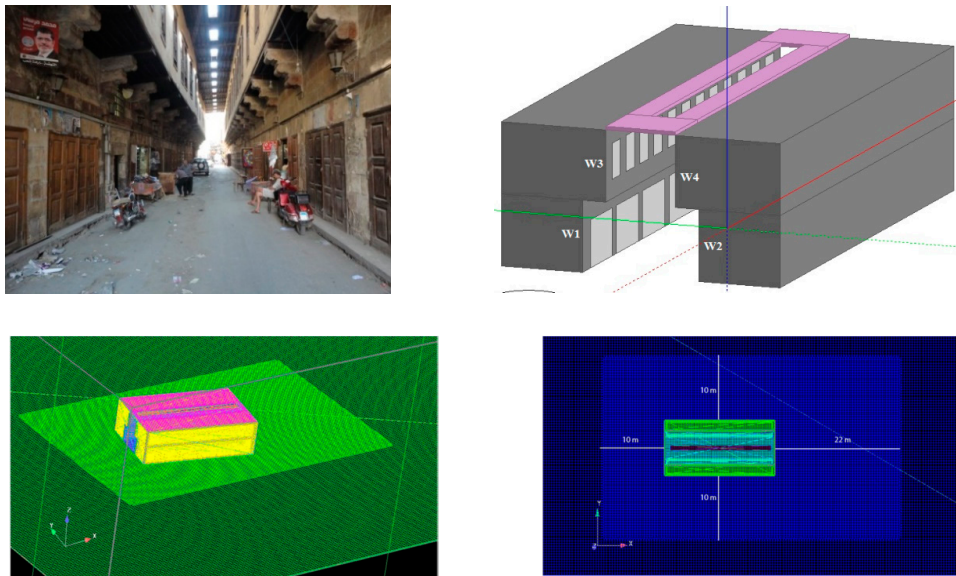


Figure 5. The meshing domain for the existing case, with the coarsened area 10 m above the model.

3. Results and Discussion

3.1. The Thermal Sensation Votes

Due to the variations in the microclimatic parameters between day and night, the inhabitants' thermal perceptions were examined based on the interviewees' thermal sensation votes in relation to the calculated PET. According to Fanger's theory [62], only votes of -1 , 0 , and $+1$ represent satisfaction with the thermal environment. The interviews were conducted with respondents who were predominantly local people living or working in the area, with an outdoor staying time of more than 20 min. As shown in Figure 6, a high percentage of respondents who voted for the three central TSV categories occupying Al Khayamiya Alley were satisfied with the thermal environment, where the thermal satisfaction levels were higher during the daytime recording 61% of the total sample compared to 51% during the night-time.

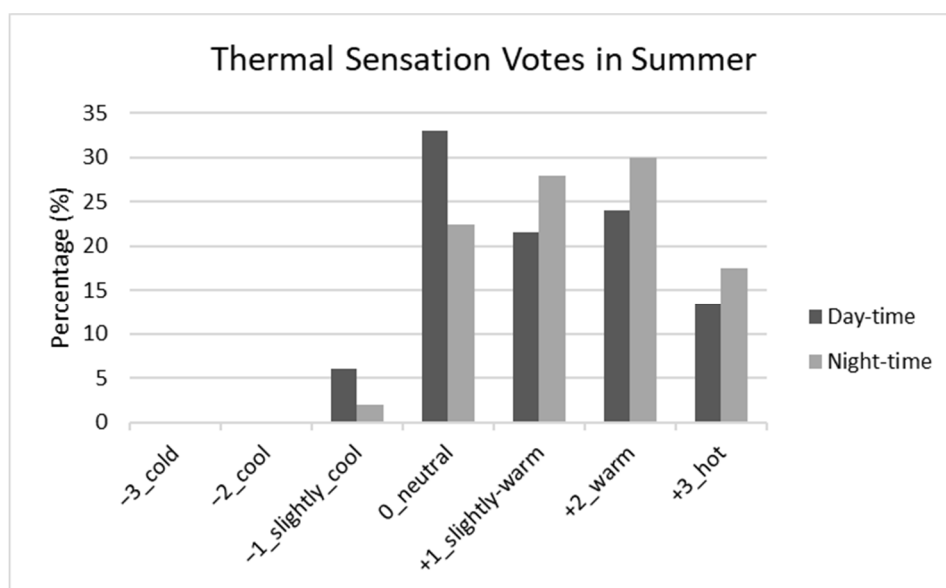


Figure 6. Subjective thermal sensation votes in daytime and night-time in the summer.

This might be explained by the existing shading settings, which improve heat stress during the day with a high level of shielding from direct solar radiation, but cause discomfort at night due to the low sky view factor, which delay or obstruct night purge [34,38].

3.2. Thermal Perception and Neutral PET

As illustrated in Figure 7, people's thermal sensations within the alley were further investigated using the ordinal logistic regression model (OLRM), which is a common method of modelling the relationship between thermal sensation and various factors.

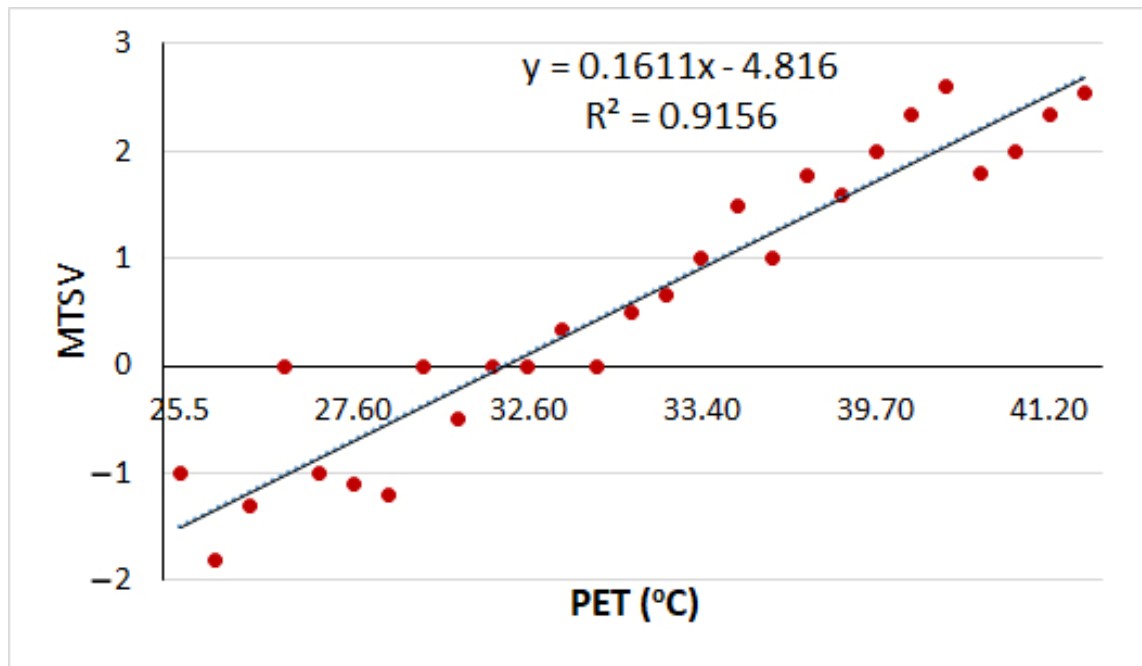


Figure 7. Correlation between actual physiological equivalent temperature (PET) and thermal sensation votes in Al Khayamiya Alley.

A simple linear regression was used for the mean TSV for each 1 °C degree PET interval. This produced Equation (7), regarding the summer season and describing the correlation between the mean thermal sensation votes (MTSVs) and PET.

$$\begin{aligned} \text{MTSV (summer shaded)} &= 0.1611 (\text{PET}) - 4.816 \\ R^2 &= 0.9156 \end{aligned} \quad (7)$$

Neutrality was derived by solving the MTSV of zero. The neutral PET is the thermal point at which people feel thermally neutral (neither cool nor warm). Neutral PET was derived by solving the MTSV of zero in the previous equations (Table 2).

Table 2. PET at different levels of thermal sensation (only votes of −1, 0, and +1 represent satisfaction with the thermal environments [62]).

MTSV	Thermal Sensation	PET (°C) Summer
−3	Cold	<17.6
−2	Cool	17.6
−1	Slightly cool	19
0	Neutral	30.1
1	Slightly warm	36
2	Warm	42
3	Hot	>42

The linear regression revealed a strong relationship between perceived comfort and PET for all cases, where the R^2 is 0.92. The neutral PET is 30.1 °C under the shade. According to a previous study in a similar context, neutral PET was 29 °C in summer for exposed areas [16]. By referring to Fanger’s theory [62], it can be assumed that subjects who only votes of −1, 0, and +1 represent satisfaction range with the thermal environment, which, in this case, varies between the PET value of 19 to 36 °C. This can be explained by people’s tendency to accept a higher temperature under shaded locations more willingly than in sun exposed ones [28]. In another study, it was found that people with a higher degree of control over their source of discomfort tolerate wide variations, and negative emotional responses are greatly reduced [63]. This may be true of the current study, as the occupants could avoid intense solar radiation by seeking available shade.

3.3. Correlation between Thermal Response Votes and Microclimatic Parameters

The correlation between the thermal sensation votes and the other environmental parameters of air temperature, wind velocity, and solar exposure were all recorded and analysed using Spearman’s Rank Order Correlation Coefficient. This quantifies the strength and direction of association between two variables measured on at least an ordinal scale [64], to identify the most significant impact regarding outdoor thermal comfort. According to Table 3, sun exposure was the predominant stimulus on people’s TSV with a correlation coefficient of 0.680, followed by air temperature (0.51).

Table 3. Correlation analysis of thermal response votes.

		TSV	Air Temperature	Wind Speed	Sun Exposure
TSV	Correlation	1	0.51 ^a	−0.179 ^a	0.680 ^a
	coefficient significant (2-tailed)	-	0.000	0.000	0.000
	N	100	100	100	100

^a correlation is significant at the 0.01 level (2-tailed).

Wind velocity had less effect on TSV, counting for a small correlation coefficient of −0.179. The findings indicate that people’s TSVs seemed to increase with an increase in the sensation of sun exposure, followed by air temperature, and a decrease, with an increase in wind speed.

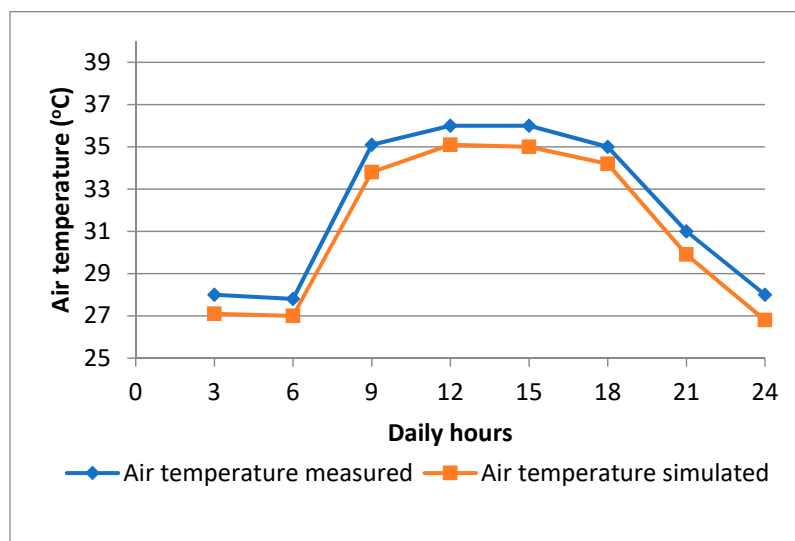
3.4. CFD Simulations: Validation and Comparative Results

3.4.1. The CFD Model Validation Results

The simulated CFD air temperature was validated against reported data from the field measurements, and the full set of data, in addition to the wall surface temperature, as presented in Figure 5. The data used as input in the CFD simulation, in addition to the simulated and the measured air temperature in the middle of the alley, are presented in Table 4, and the validation results at three-hour intervals were plotted for better illustration, as shown in Figure 8.

Table 4. Validation of air temperature taken at the middle of the alley in addition to model input of surface temperatures.

Time Intervals	For Validation Purposes		Simulation Inputs					
	Hours	Measured	Simulated Outcomes	Wall 1	Wall 2	Wall 3	Wall 4	Roof
		Air temperature (°C)		Surface temperature (°C)				
3.00	28.0	27.1	26.8	27.5	27.4	27.0	31.1	
6.00	27.8	27.0	26.3	27.6	26.8	27.7	30.2	
9.00	35.1	33.8	28.0	30.3	28.6	35.9	33.2	
12.00	36.0	35.1	30.6	31.7	31.6	32.9	37.7	
15.00	36.0	35.0	33.0	32.6	39.0	33.9	39.2	
18.00	35.0	34.2	32.8	31.8	35.7	32.4	36.7	
21.00	31.0	29.9	29.5	30.0	30.8	29.9	34.1	
24.00	28.0	26.8	28.5	29.1	29.4	28.8	32.5	

**Figure 8.** Actual measured air temperature under the shaded roof against CFD simulation output at pedestrian level for validation purposes.

The CFD outcomes displayed a consistent trend against the field measurements, with small differences varying between 0.8 °C–1.2 °C. This indicates the ability of the designed model to address the existing pattern of air temperature in the current study, and, in turn, provides some confidence in applying the same settings to examine the iterations for the suggested shading scenarios.

3.4.2. Comparative Results

As per the BPG, the same settings used for the validations were applied to the test scenarios, and then a cross-comparison of the impact of each scenario was observed, including the air temperature distribution, natural ventilation performance, and effect on outdoor thermal conditions. The six tested scenarios, as presented in Figure 3, were all directed on the same track as the prevailing wind direction, and each scenario was based on a certain geometric change regarding the roof shape and opening positions. The boundary conditions were adjusted based on the same date as the validation to represent a typical summer day, and simulation was adjusted to night-time. As stated, the high level of shading elevates thermal comfort during summer days, but at night, reduces the long wave radiation loss rate on surfaces, causing a higher temperature compared to unshaded sites [30,38,65].

3.4.3. Comparison of the Vertical Profiles of Mean Wind Velocity

To investigate wind speed effect at the pedestrian level, a vertical profile representing the mean wind velocity was located in the middle of the alley. The profile is 7 m tall from ground level to the top of the roof, with a wind speed reference of 3 m/s at 10 m height, as shown in Figure 9.

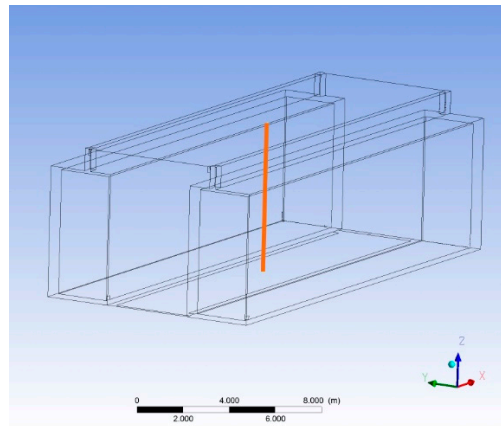


Figure 9. Vertical profiles located in the centre of the alley facing the prevailing wind route.

According to the measurements taken along the vertical profiles (Figure 10 and Table 5), all cases share similar profiles at lower levels before they are very close to the opening levels, and then the profiles' contour lines start to vary.

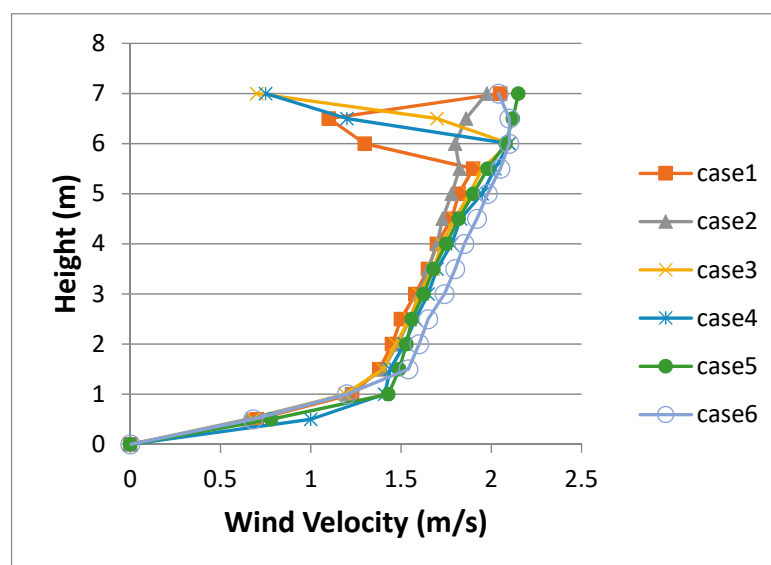


Figure 10. Simulated mean wind velocities located at the 7 m height vertical line centre alley.

In the first two cases, they have almost the same values and vertical contours for wind speed, until 1 m under roof level. Case 1's wind velocity went down to 1.1 m/s, from 1.9 m/s, where the rooftop is solid, with no openings, before it reaches, again, 2 m/s above the roof. Case 2 has a centred rooftop opening that released the wind slightly slower, at about 0.05 m/s. However, in cases 3 and 4, the side openings caused a greater reduction in wind velocity by enabling its release from both sides. Both cases have two side openings, but with different locations, as shown in Figure 3, and this appeared to have a negligible effect on wind speed or the profile underneath, as both cases reported an equal maximum wind velocity of 2.1 m/s, and almost equal rates at roof level of 0.70 m/s and 0.75 m/s, respectively. For cases 5 and 6, which have one more opening in the centre of the roof than the previous two cases,

their greater number of openings and locations assisted wind release, while maintaining wind speed. Both cases had the same vertical contours regarding average wind velocity along the whole profile and, as a result, the number and location of the openings in the shading surface is crucial to shaping the wind speed and profile underneath.

Table 5. Simulated mean wind velocity outcomes for each case along the 7 m vertical profile.

Height	Case 1	Case 2	Case 3	Case 4	Case 5	Case 6
m	Velocity (m/s)					
0	0	0	0	0	0	0
0.5	0.7	0.65	0.68	1	0.78	0.68
1	1.23	1.2	1.19	1.41	1.43	1.2
1.5	1.38	1.4	1.4	1.44	1.49	1.54
2	1.45	1.48	1.47	1.52	1.53	1.6
2.5	1.5	1.55	1.55	1.58	1.56	1.65
3	1.58	1.6	1.6	1.65	1.625	1.74
3.5	1.65	1.65	1.68	1.7	1.68	1.8
4	1.7	1.7	1.725	1.78	1.75	1.85
4.5	1.78	1.73	1.8	1.83	1.82	1.92
5	1.82	1.78	1.88	1.95	1.9	1.98
5.5	1.9	1.825	1.95	2.02	1.98	2.05
6	1.3	1.8	2.1	2.1	2.08	2.1
6.5	1.1	1.86	1.7	1.2	2.12	2.1
7	2.05	1.975	0.7	0.75	2.15	2.04

These findings match well with a preceding study stating that urban geometry is mainly responsible for wind behaviour at pedestrian level, and not building height, which significantly influences the wind environment on a larger scale [66] (Ng et al., 2011). A study by Ng et al. [67] on achieving urban thermal comfort with wind speed threshold values at pedestrian level in hot regions, for a typical summer's day, a wind speed range of 0.6–1.3 m/s was required to achieve neutral thermal sensation (neutral PET: 28.1 °C). Another study for the same climate conditions found that 1.6 m/s wind speed was required to achieve outdoor thermal comfort [68]. Yuan and Ng [69] proposed five different categories for pedestrian-level wind speed in a street canyon, as presented in Table 6.

Table 6. Classification of pedestrian-level natural ventilation (u) in street canyons [69].

Class 1	$U < 0.3$ m/s	Stagnant
Class 2	0.6 m/s $> u \geq 0.3$ m/s	Poor
Class 3	1.0 m/s $> u \geq 0.6$ m/s	Low
Class 4	1.3 m/s $> u \geq 1.0$ m/s	Satisfactory
Class 5	$U \geq 1.3$ m/s	Good

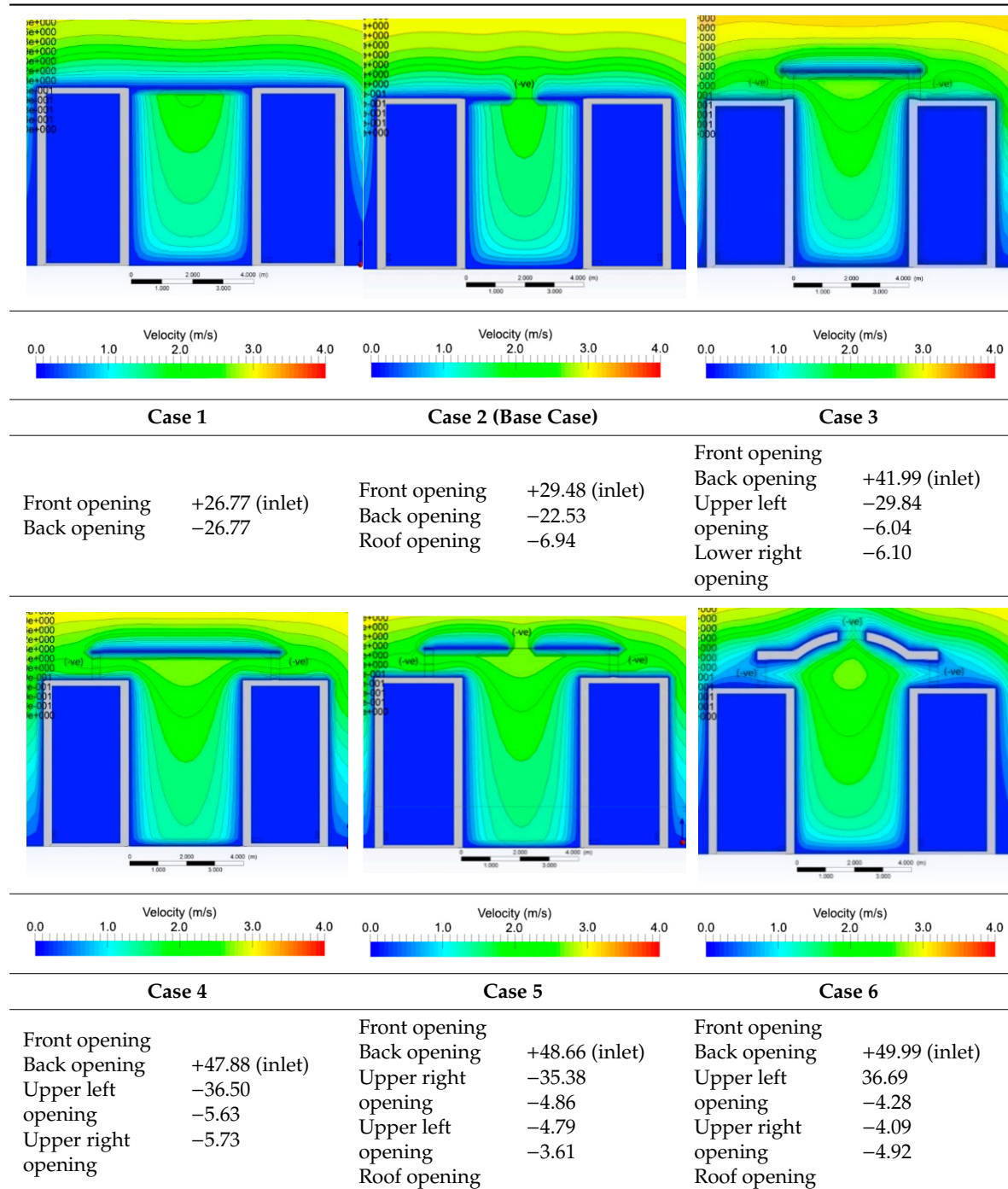
Based on these results, all of the examined cases in the current study fall within the fifth class of wind speed ≥ 1.3 m/s, achieving thermal comfort by natural ventilation. Case 6 represents ideal conditions by recording 1.6 m/sec, according to the recommendations of Cheng et al. [68]. However, the outdoor environment is heterogeneous, and relying alone on wind velocity for describing thermal comfort is not enough, therefore, the study used the wind velocity outcomes for each case to calculate the PET as the main comfort index in the later section.

3.4.4. The Ventilation Flow Rate

According to Hang et al. [70], the effect of semi-open street roofs on the natural ventilation underneath is less understood as it may produce various flow patterns and ventilation capacities. Therefore, it was very important to quantify the effects of the roof opening on the ventilation by quantifying the flow rate. Table 7 presents the normalised flow rates (Q^*) for the examined case studies,

where the positive values represent the incoming air and the negative values denote the existing air, while Figure 11, shows the overall performance of the flow rates for each case.

Table 7. Volumetric flow rate (Q) (m³/s) through the alley’s openings. Positive Q values refer to air entering (inlet) and negative values denote air leaving (outlet).



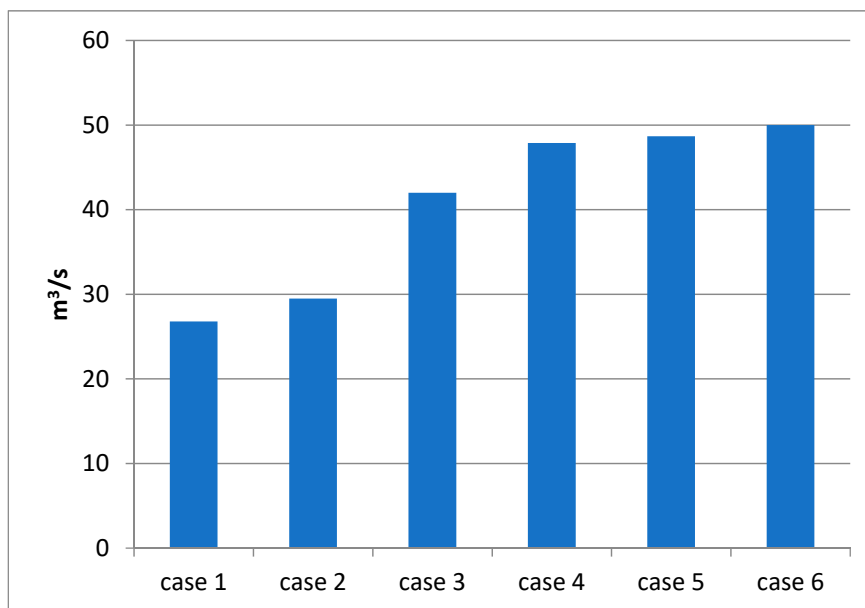


Figure 11. Total volume flow rate (m³/s).

Although cases 1 and 2 have an equal space volume of 464 m³, it was found that case 2 had 10% more flow rate than case 1 due to the roof opening accounting for 23.5% of the entire flow rate.

Regarding cases 3 and 4, the latter recorded a higher flow rate due to its slightly greater volume space compared to the former, but the two-sided roof opening in these cases both accounted for 30% of the total ventilation flow rate. Again, by assessing cases 4 and 5, which shared the same volume, case number 5—with an extra opening in the centre of the roof—accounted for only a 2% higher volume rate than case 4. In cases 5 and 6, both have the same top opening numbers and locations, but a different roof shape (case 5 has a flat roof and 6 a vaulted shape). Both cases recorded the same amount of total volume rate of 27%, and yet the top centre opening in case 6 was responsible for 10% of the total volume flow rate, compared to 7.4% for case 5. This improved the volume flow by 2.8% for case 6 against case 5, possibly because of the roof shape. It has been suggested that vault-shaped roofs increase the inflow rate and redistribute the internal airflow by directing some of the air to exit through the roof openings instead of the wall openings [71].

3.4.5. Comparison of Air Temperature Distribution

The same vertical profile settings used to examine the mean wind velocity were applied to the analysis of the mean air temperature, with 35 °C being the reference air temperature at the inlet as reported in the in situ field measurements. Table 8 and Figure 12 represent the mean air temperature profiles for the six cases.

Each simulated mean air temperature profile was about 7 m high, starting from ground level to the top of the roof. All of the examined cases had mean air temperatures varying between 32.4 °C and 33.4 °C at the ground level (Table 8), with only a 1 °C difference between all cases. These values were lower than the inlet air temperature, possibly due to the ventilation flow rate and shading effect. The situation changed as the mean air temperature difference started to increase. Case 1 had the highest temperature, followed by cases 2 and 3, with a slight difference of less than 0.2 °C. Although these cases have similar vertical profile contours, close to the roof level, case 1 had a slight increase in air temperature, while in case 3—with two side openings—the air temperature had the same increase as case 1, before falling again at the side opening level. When comparing the profile trend of cases 4 and 5, both had very similar air temperature distribution by profile, but case 5 had an extra opening mid roof, which gave the indication that the centre location of the opening may have had less influence on air temperature distribution than wind velocity. Although case 6 had the same number and location of

openings as case 5, it was noted that it had the lowest air temperature along the vertical line compared to other cases. In this case, the air temperature suddenly increased by 1.5 °C once it reached the side opening level, to reach the inlet temperature of 35 °C. This may refer to the mode of heat transfer from the semi-closed space to the outside air temperature [72]. The air temperature dropped again by the same amount (1.5 °C) right under the roof top. This variation in air temperature between cases 5 and 6 may be due to the vaulted shape in case 6, as the top roof centre opening seemed to have no effect on the air temperature underneath, as mentioned previously. Hence, case 6 may be the best of the examined scenarios for having the lowest air temperature, especially at pedestrian level, as the difference in air temperature was 1 °C compared to cases 4 and 5, and 1.6 °C compared to case 2. This may be explained by Hadavand and Yaghoubi [73], as in their study the vaulted shape received less solar heat per unit area due to the curved shape, which in turn lowered surface temperatures, and assisted heat reradiation after sunset. In addition, heat transmission by vaulted or curved roofs to the interior is reduced compared to flat ones [74]. Overall, air temperature in the current study was directly proportional to the height of the profile, and there was a direct proportional relationship between air temperature and profile level; that is, the higher the level, the higher the air temperature, until the air reached the side openings, when the air temperature reached its peak due to the direct interaction with the outside air temperature. This warm air migration to the top of the semi-enclosure offers possible solutions for more comfortable adjustment, resulting in the availability of cooler air at the ground level in the pedestrian zone. In addition, the hot air reservoir at higher levels may have been discharged through the upper level opening and, thus, generated a cooling airflow at lower levels, steered by the stack effect [72].

Table 8. Simulated mean air temperature (°C) outcomes for each case along the 7 m vertical profile.

Height	Case 1	Case 2	Case 4	Case 4	Case 5	Case 6
m	Air Temperature (°C)					
0	32.5	33.4	33.3	32.5	32.8	32.4
0.5	33.6	33.7	33.5	33.5	33.4	32.7
1	34.5	34.7	34.5	33.9	33.9	32.9
1.5	34.6	34.8	34.6	34.1	34.0	33.1
2	34.7	34.8	34.7	34.1	34.1	33.1
2.5	34.7	34.8	34.7	34.2	34.2	33.1
3	34.7	34.8	34.7	34.2	34.2	33.2
3.5	34.8	34.9	34.8	34.3	34.3	33.2
4	34.8	34.9	34.8	34.3	34.3	33.3
4.5	34.8	34.9	34.8	34.4	34.4	33.3
5	34.8	34.9	34.8	34.5	34.5	33.3
5.5	34.9	34.9	34.9	34.5	34.5	33.4
6	34.9	34.9	34.9	34.7	34.7	34.4
6.2	34.9	34.9	34.9	34.8	34.8	34.9
6.5	34.9	34.9	34.9	34.6	34.5	34.2
7	35.0	35.0	34.8	34.0	34.0	33.5

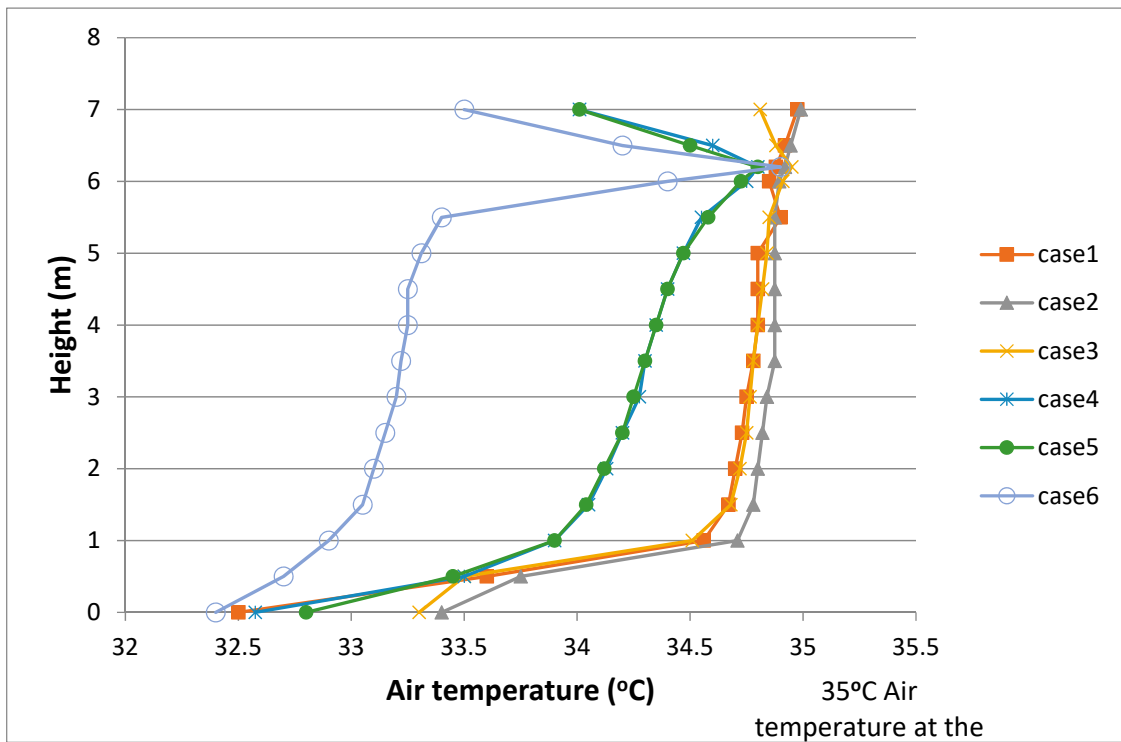


Figure 12. Simulated mean air temperature at the 7 m height vertical line in the alley centre.

Moreover, by examining the relationship between the mean air temperature and the previous analysis regarding wind velocity, a negative correlation was found, where an increase in wind speed would be equal to a reduction in the air temperature and vice versa (Figure 13).

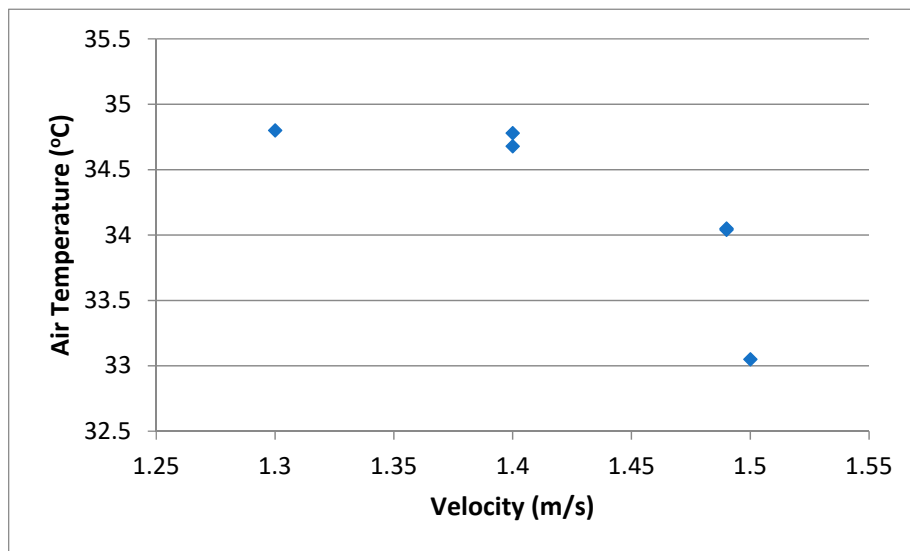


Figure 13. Relationship between mean air temperature and wind velocity at pedestrian level.

Similar outcomes were found in previous studies [67–69,75,76].

3.4.6. Mean Radiant Temperature and PET

Relying on wind velocity and air temperature alone to evaluate overall thermal comfort is insufficient, and it is essential to apply a thermal comfort index using the main microclimate parameters as described in the ASHRAE Standard [43]. Therefore, as a comfort index, the physiologically

equivalent temperature (PET) [77,78] was calculated for each case using the Rayman model [79,80] and the simulation output for the dominant microclimatic parameters. The exception to this was mean radiant temperature, which was calculated for each case based on the following equation ASHRAE [45], Equation (8):

$$T_{mrt} = \left[(T_g + 273.15)^4 + \frac{1.1 \times 10^8 V_a^{0.6}}{\varepsilon_g D^{0.4}} \times (T_g - T_a) \right]^{\frac{1}{4}} - 273.15 \quad (8)$$

(T_g) is the globe temperature ($^{\circ}\text{C}$), (V_a) is air velocity (m/s), (T_a) is the air temperature ($^{\circ}\text{C}$), D (mm) is the globe diameter (=25 mm), and (ε_g) is the emissivity of the sphere (=0.95 for a black globe).

All of the parameters for Equation (8) were available except for the globe temperature (T_g), which had to be recalculated using the simulation outcomes for air temperature and wind velocity in each case, by applying the following equation [81,82], Equation (9):

$$T_g = \frac{B + CT_a + 7680000}{C + 256000} \quad (9)$$

where, (T_a) is air temperature and B and C are defined as, Equation (10):

$$B = S \left(\frac{f_{db}}{4 \sigma \cos(z)} + \left(\frac{1.2}{\sigma} \right) f_{dif} \right) + (\varepsilon_a) T_a^4 \quad (10)$$

$$C = \frac{hv^{0.58}}{(5.3865 \times 10^{-8})} \quad (11)$$

where, (T_a) is air temperature ($^{\circ}\text{C}$), (σ) the Stefan–Boltzmann constant = 5.67×10^{-8} , (S) solar irradiance, (f_{db}) direct beam radiation from the sun, (f_{dif}) diffuse radiation from the sun, (z) solar angle to zenith, (s) solar irradiance (W/m^2), (h) convective heat transfer coefficient, (v) wind velocity (mph) and (ε_a). According to Hunter and Minyard [83], thermal emissivity can be calculated using the following, Equation (12):

$$\varepsilon_a = 0.575ea^{\left(\frac{1}{7}\right)} \quad (12)$$

where, (ea) is atmospheric vapour pressure.

Equation (2) calculates globe temperature, according to an experiment by Dimiceli et al. [81,82], in which output variations vary within 0.27°C between measured and estimated temperatures.

All of the data used in the equation, in addition to the globe, mean radiant temperature, and PET, are presented in Table 9.

Table 9. Values used to calculate globe temperature (T_g), mean radiant temperature (T_{mrt}) and PET, in addition to the constant values used in Equations (9)–(12).

Parameters	Case 1	Case 2	Case 3	Case 4	Case 5	Case 6
v (m/s)	1.38	1.4	1.4	1.45	1.49	1.54
T_a	34.67	34.78	34.68	34.05	34.04	33.05
B	2,668,708.03	2,702,738.3	2,671,788.3	2482871	2,479,955.6	2,203,796.82
C	783,414,319	789,979,636	789,979,636	806,222,801	819,048,598	834,879,223
T_g	34.67	34.78	34.68	34.05	34.04	33.05
T_{mrt}	34.75	34.84	34.79	34.16	34.15	33.06
PET	35.2	35.2	35.1	34.2	34.2	32.9
Constant Values Used in Equations (9)–(12)						
z	90.22		s	0 (at night)		f_{db} 0
ea	22.48619		h	0.127660528		f_{dif} 100

Some variables are the same for all cases, including the vapour pressure, solar angle to zenith, and solar irradiance, as the examined cases share the same conditions and location. Based on the

calculated PET and the acceptable range calculated previously from the survey, none of the six scenarios successfully reached the acceptable range. However, case six achieved a reduction in PET of 2.3 °C compared to the base case, followed by cases 4 and 5 with 1 °C differences. These differences in the comfort range were designated slightly warm, as per the PET classification, and this only came from the shading parameter. Nevertheless, by adding different parameters, such as vegetation [84,85], type of materials, and albedo [86–88], a further reduction and better comfort range is expected.

3.4.7. Outputs Reflection on Psychometric Chart

To predict the performance of various shading scenarios on urban thermal comfort, analysis of measured field data is triangulated with subjective survey responses and computational Fluid Dynamics (CFD-ANSYS) modelling. A summary of the results of iterations of the shading scenarios to the base case are presented in Table 10. Table 10 shows changes to air temperature, air velocity, and PET.

Table 10. The final environmental outcomes and PET comfort index for all the examined case studies.

Cases	Volume Flow Rate	Air Velocity	Air Exchange Rate	Air Temperature	PET
	(m ³ /s)	m/s	m ³ /h	(°C)	(°C)
1	26.77	1.38	207.7	34.67	35.2
2 Base Case	29.48	1.4	228.7	34.78	35.2
3	41.99	1.4	277.8	34.68	35.1
4	47.88	1.45	295	34.05	34.2
5	48.66	1.49	299	34.04	34.2
6 Best Case	49.99	1.54	300	33.05	32.9

Results indicate the mutual relationship between changing the roof shape and its openings on environmental parameters affecting thermal comfort and the cooling effect for the pedestrians at street level. Results indicate the best reductions of 2.3 °C in air temperature and 32.9 °C as PET can be achieved when the roof configuration is vaulted with central and side openings (Case 6), compared to air temperature of 34.8 °C and PET 35 °C recorded when the roof configuration is flat and with one centre opening (Case 2). Applying the simulation results on a psychometric chart will make it easier to link between the best and base case, in accordance to the neutral PET and comfort range developed from the in situ field measurements and questionnaire survey on phase one.

Firstly, Figure 14 presents the thermal comfort acceptable range and neutral PET according to the estimates from the in situ field measurements and the subjective questionnaire, in addition to the PET obtained from the CFD modelled cases.

Plotting results of this study from the field measurements and survey on the (ISO 7730:2005) [89] for thermal comfort psychometric chart, considering relative humidity in Cairo ranges between 40 and 60% year-round, it can be concluded that people of the examined site express a wider range of comfort, compared to the ISO 7730 scale (Figure 15).

This confirms that people who live in hot arid climates have a wider range of adaptation and tolerance to local climatic conditions year-round, compared to the range suggested by the standard for moderate climate conditions. Similar studies have reported the same conclusion, such as, Lin [90], who examined the outdoor thermal comfort in a hot and humid subtropical climate, where the PET acceptance range was 21.3–28.5 °C, higher when compared to a European scale of 18–23 °C PET. Cohen et al. [22] also reported the same regarding the Mediterranean climate, as the PET values were higher by 3 °C than the European scale. Moreover, Elnabawi et al. [16] reported a thermal comfort range of 23–32 °C PET for a hot arid climate, which was found to be higher than both temperate and humid subtropical climate acceptance range. This supports the claim of many scholars that thermal comfort indices established in temperate areas are unsuitable to be applied elsewhere. Local subjective comfort data acquired for the examined site incorporated in predictive comfort studies provides a better assessment of outdoor thermal comfort representing the locals who are in regular contact with the space [16,22,28].

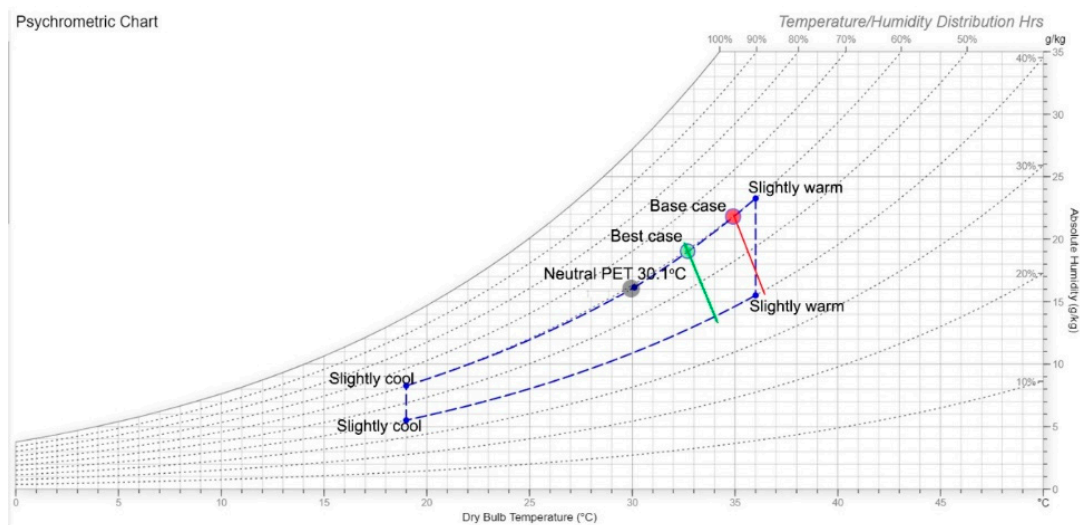


Figure 14. Case study psychrometric chart for outdoor thermal comfort acceptable range and neutral PET according to the estimates from the in situ field measurements and the subjective questionnaire, in addition to the PET obtained from the CFD modelled cases.

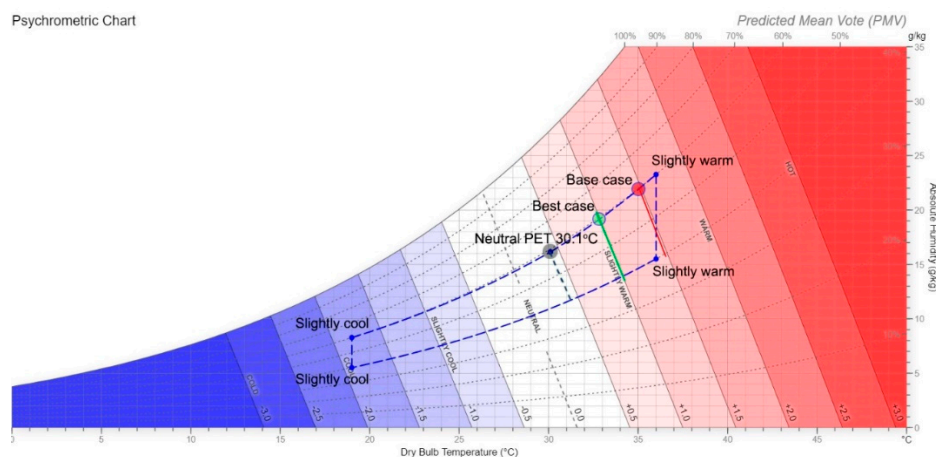


Figure 15. Psychrometric chart summarises the study outputs where the comfort range (the blue dotted lines) compared against the ISO 7730:2005 [89] comfort range. The best case no. 6 (32.9 °C PET) and the base case no 2 (35.2 °C PET) are within the acceptable range however when compared to the ISO range; only the best case can be considered within the comfort range (slightly warm).

Secondly, although the maximum results of thermal comfort improvement due to changing the roof configuration did not reach the neutral PET (which is the thermal point at which people feel thermally neutral), it still predicted a PET reduction of 2.3 °C compared to base case conditions (35.1 °C). This reduction moves comfort sensation predictions according to estimated ones, and the ISO 7730 [89] comfort range (slightly warm), from warm zone for the base case to slightly warm conditions for the best case, which falls within the acceptable comfort range.

4. Conclusions

Human thermal comfort in outdoor spaces in hot arid regions may depend as much on the radiant load to which a pedestrian is exposed as to air temperature. Accordingly, scholars have found that shade plays the main role in tackling outdoor discomfort in hot arid climates, especially in summer [12,28,30–33]. Applying any type of shading form or arrangement within an existing urban site influences other microclimatic parameters, and most likely affects thermal perception and comfort.

Few studies have provided an in-depth analysis that considers multiple types of shading strategies [35]. Therefore, the comprehensive framework considered in this study, which integrates quantitative and qualitative parameters, and links these to the microclimatic environment with a subjective thermal assessment, adds to the field. This framework works on two levels; the first includes the on-site field measurements accompanied by the field survey, for which the following findings were recorded:

- The percentage of people satisfied with the thermal environment during the day (61%) was more than those satisfied with the thermal conditions during the night (51%). This may be explained by the performance of the shading elements, which assist in reducing the amount of direct solar radiation. This results in reduced heat released from the surrounding surfaces, reducing air temperature during the day; however, at night, these shading elements obstruct the accumulated heat underneath the shading system from release, causing a delay in heat release and boosting the UHI effect [65];
- Direct solar radiation is the dominant microclimatic parameter in shaping people's thermal perceptions, with a correlation coefficient of 0.680 (Table 2);
- Neutral PET was 30.1 °C under the shade on summer days.

Based on outcomes, such as the microclimatic parameters from the field measurements, and the actual TSV and PET from the field survey, the framework incorporates numerical modelling and parametric analysis as a subsequent level. The study examined six different shading scenarios using CFD, addressing the type of shape and number of openings and their locations within the shading elements. In so doing, the study examined the overall thermal performance underneath, based on dependent variables of air temperature and wind velocity distributions, ventilation flow rate, and the PET. The findings at this level are summarised as follows:

- The shading form and opening location proved to influence the wind vertical profiles underneath. The analysis showed that the wind profiles for the examined scenarios tended to follow similar patterns, starting from the ground level until they became close to the opening levels, at which point each profile started to have its own shape and speed based on the opening location or the roof shape;
- The shading device shapes and opening locations were dominant features in causing a reduction in air temperature within the urban scale. This alteration in the shading form led to a reduction of 2.3 °C in air temperature for the best case, case 6;
- A positive relationship was found between the air temperature vertical distribution and the profile levels, where the higher the level, the higher the air temperature. This migration of the stratified hot air to the roof top and the shading devices may be a possible solution for more comfortable adjustments, resulting in the availability of cooler air at the ground level in the pedestrian zone. In addition, the hot air reservoir at higher levels may be discharged through the upper level opening and, thus, generate a cooling airflow at lower levels, steered by the stack effect [72];
- A negative correlation was found between the wind velocity and the air temperature underneath, since there is a reduction in the air temperature when the wind velocity increases, and vice versa. This relationship was expected as it has been reported previously in several studies [68,69,75,76];
- In terms of ventilation flow rate, both the number and location of openings was found to be the key to better performance. The cases with side and roof openings showed an increase in ventilation volume rate of 23–30% compared to those with roof or side openings;
- Again, in terms of ventilation, the use of a vaulted roof increases the inflow rate (10%) compared to a flat roof (7.4%). According to Asfour and Gadi [71], the vaulted roof can be used to improve the natural ventilation underneath as it redistributes the internal air flow by attracting some air to leave through the top opening in the roof;
- The vaulted shape proved to receive less solar heat per unit area due to the curved shape, which in turn led to lower surface temperatures; it thus assists reradiation after sunset [73], and additionally

the heat transmission of a vaulted or curved roof to the interior is reduced compared to flat ones [74];

- All of these factors led to a reduction in overall thermal comfort (PET), as the best case with the vaulted roof (case 6) recorded 32.9 °C compared to 35.2 °C for the Base Case (case 2), which is 2.9 °C from neutral or accepted PET and within three central votes of thermal satisfaction [62];
- The reduction in air temperature was due to the vaulted shape of the roof with three openings, as it causes a higher air velocity and higher air exchange rate underneath, which has a positive effect in decreasing the air temperature. Moreover, the vault shaped roof with its curved surface area is considerably larger than the base case roof with no openings, and so receives less solar heat per unit area; thus, lowering surface temperatures and facilitating reradiation after sunset. The vaulted configuration continuously, this process improved the thermal comfort of the pedestrian area, as the PET for the best case 6 was about 32.9 °C against 35 °C for the base case, which was only 0.9 °C, close to the thermal acceptable range on the hottest day of the year.

In conclusion, the paper proposes a comprehensive interdisciplinary framework that can correlate between the different levels of assessment, including objective assessments, such as in situ field measurements and subjective ones, including questionnaires and site observations, which proved to be very reliable methods in tackling the thermal comfort, defined as state of mind that expresses satisfaction with the surrounding environment, indicating that comfort is a physiological and psychological condition. Accordingly, thermal comfort has been examined solely, from either a physical or psychological point of view, without any serious attempt to correlate and impose these results into urban design proposals.

Therefore, based on the calculated and calibrated comfort index obtained from the site measurements and social survey. The first three objectives in Section 2 (methodology) have been achieved. However, when this comfort index was taken to the next phase in an attempt to correlate between the social and psychological level of assessment obtained from phase one, with the design level of phase two, by acquiring the parametric modelling for different shading scenarios based on the previously calculated PET and acceptable range, none of the scenarios successfully reached the acceptable range. However, the outcomes were very promising, where one of the scenarios achieved a 2.3 °C reduction of the PET compared to the base case, which definitely opens the door for more studies, for testing more shading scenarios, or adding more parameters, such as vegetation [84,85], type of materials, albedo [86–88], and some active techniques, where a further reduction and better comfort range is expected, as well as testing more frameworks, including different levels of assessment in relation to the design.

Author Contributions: Conceptualization, M.H.E. and N.H.; Formal analysis, M.H.E.; Investigation, M.H.E.; Methodology, M.H.E. and N.H.; Supervision, N.H.; Writing—review and editing, M.H.E. and N.H. All authors have read and agreed to the published version of the manuscript.

Funding: This research received no external funding.

Conflicts of Interest: The authors declare no conflict of interest.

References

1. IPCC. *Global Warming of 1.5 °C*; Masson-Delmotte, V., Zhai, P., Pörtner, H.-O., Roberts, D., Skea, J., Shukla, P.R., Pirani, A., Moufouma-Okia, W., Péan, C., Pidcock, R., et al., Eds.; IPCC: Geneva, Switzerland, 2018; in press.
2. Harlan, S.H.; Brazel, A.J.; Prashad, L.; Stefanov, W.L.; Larsen, L. Neighborhood microclimates and vulnerability to heat stress. *J. Soc. Sci. Med.* **2006**, *63*, 2847–2863. [[CrossRef](#)] [[PubMed](#)]
3. Adam-Poupard, A.; Labrèche, F.; Smargiassi, A.; Duguay, P.; Busque, M.A.; Gagné, C.; Rintamäki, H.; Kjellstrom, T.; Zayed, J. Climate change and Occupational Health and Safety in a temperate climate: Potential impacts and research priorities in Quebec, Canada. *Ind. Health* **2013**, *51*, 68–78. [[CrossRef](#)] [[PubMed](#)]
4. Tibbetts, J.H. Air quality and climate change: A delicate balance. *Environ. Health Perspect.* **2015**, *123*, A148–A153. [[CrossRef](#)] [[PubMed](#)]

5. Santamouris, M.; Papanikolaou, N.; Koronakis, I.; Georgakis, C.; Argiriou, A.; Assimakopoulos, D.N. On the impact of urban climate on the energy consumption of buildings. *J. Sol. Energy* **2001**, *70*, 201–216. [[CrossRef](#)]
6. Gartland, L. *Heat Islands Understanding and Mitigating Heat in Urban Areas in the UK and USA in 2008*; Earthscan: London, UK, 2008.
7. Lee, K.; Kim, Y.; Chan Sung, H.; Ryu, J.; Woo Jeon, S. Trend analysis of urban island intensity according to urban area change in Asian Mega Cities. *Sustainability* **2020**, *12*, 112. [[CrossRef](#)]
8. Roth, M. Effects of cities on local climates. In Proceedings of the IGES/APN Mega-City Project, Kitakyushu, Japan, 23–25 January 2002.
9. Jarah, S.H.A.; Zhou, B.; Abdullah, R.J.; Lu, Y.; Yu, W. Urbanization and Urban Sprawl Issues in City Structure: A Case of the Sulaymaniah Iraqi Kurdistan Region. *Sustainability* **2019**, *11*, 485. [[CrossRef](#)]
10. Lee, H.; Holst, J.; Mayer, H. Modification of Human-Biometeorologically Significant Radiant Flux Densities by Shading as Local Method to Mitigate Heat Stress in Summer within Urban Street Canyons. *Adv. Meteorol.* **2013**, *2013*, 312572. [[CrossRef](#)]
11. Shishegar, N. Street Design and Urban Microclimate: Analyzing the Effects of Street Geometry and Orientation on Airflow and Solar Access in Urban Canyons. *J. Clean Energy Tech.* **2013**, *1*, 52–56. [[CrossRef](#)]
12. Middel, A.; Häb, K.; Brazel, A.J.; Martin, C.A.; Guhathakurta, S. Impact of urban form and design on mid-afternoon microclimate in Phoenix Local Climate Zones. *Landsc. Urban Plan.* **2014**, *122*, 16–28. [[CrossRef](#)]
13. Taleghani, M.; Kleerekoper, L.; Tenpierik, M.; van den Dobbelsteen, A. Outdoor thermal comfort within five different urban forms in The Netherlands. *Build. Environ.* **2015**, *83*, 65–78. [[CrossRef](#)]
14. Algeciras, J.A.R.; Coch, H.; Pérez, G.D.P.; Years, M.C.; Matzarakis, A. Human thermal comfort conditions and urban planning in hot-humid climates—The case of Cuba. *Int. J. Biometeorol.* **2016**, *60*, 1151–1164. [[CrossRef](#)] [[PubMed](#)]
15. Lindberg, F.; Thorsson, S.; Rayner, D.; Lau, K. The impact of urban planning strategies on heat stress in a climate-change perspective. *Sustain. Cities Soc.* **2016**, *25*, 1–12. [[CrossRef](#)]
16. Elnabawi, M.H.; Hamza, N.; Dudek, S. Thermal perception of outdoor urban spaces in the hot arid region of Cairo, Egypt. *Sustain. Cities Soc.* **2016**, *22*, 136–154. [[CrossRef](#)]
17. Karyono, T.H. Report on thermal comfort and building energy studies in Jakarta-Indonesia. *J. Build. Environ.* **2000**, *35*, 77–90. [[CrossRef](#)]
18. Feriadi, H.; Wong, N.H. Thermal comfort for naturally ventilated houses in Indonesia. *J. Energy Build.* **2004**, *36*, 614–626. [[CrossRef](#)]
19. Lin, T.P.; Matzarakis, A. Tourism climate and thermal comfort in Sun Moon Lake, Taiwan. *Int. J. Biometeorol.* **2008**, *52*, 281–290. [[CrossRef](#)]
20. Nikolopoulou, M.; Lykoudis, S. Thermal comfort in outdoor urban spaces: Analysis across different European countries. *J. Build. Environ.* **2006**, *41*, 1455–1470. [[CrossRef](#)]
21. Kántor, N.; Unger, J.; Gulyas, A. Subjective estimations of thermal environment in recreational urban spaces: Part 2 international comparison. *Int. J. Biometeorol.* **2012**, *56*. [[CrossRef](#)]
22. Cohen, P.; Potchter, O.; Matzarakis, A. Human thermal perception of Coastal Mediterranean outdoor urban environments. *J. Appl. Geogr.* **2013**, *37*, 1–10. [[CrossRef](#)]
23. Elnabawi, M.; Hamza, N. Behavioural Perspectives of Outdoor Thermal Comfort in Urban Areas: A Critical Review. *Atmosphere* **2020**, *11*, 51. [[CrossRef](#)]
24. OKE, T.R. *Initial Guidance to Obtain Representative Meteorological Observations at Urban Sites*; IOM Report No. 81, WMO/TD No. 1250; World Meteorological Organization: Geneva, Switzerland, 2006.
25. Fahmy, M.; Sharples, S. The Need for an Urban Climatology Applied Design Model. *Online Newsl. Int. Assoc. Urban Clim.* **2008**, *28*, 15–16.
26. Nouri, A.S.; Costa, J.P.; Santamouris, M.; Matzarakis, A. Approaches to outdoor thermal comfort thresholds through public space design: A review. *Atmosphere* **2018**, *9*, 108. [[CrossRef](#)]
27. Shooshtarian, S.; Rajagopalan, P.; Sagoo, A. A comprehensive review of thermal adaptive strategies in outdoor spaces. *Sustain. Cities Soc.* **2018**, *41*, 647–665. [[CrossRef](#)]
28. Elnabawi, M.H.; Hamza, N. A Behavioural Analysis of Outdoor Thermal Comfort: A Comparative Analysis between Formal and Informal Shading Practices in Urban Sites. *Sustainability* **2020**, *12*, 9032. [[CrossRef](#)]
29. Gehl, J. *Life between Buildings: Using Public Space*; Island Press: Washington, DC, USA, 2008.
30. Pearlmutter, D.; Berliner, P.; Shaviv, E. Integrated modeling of pedestrian energy exchange and thermal comfort in urban street canyons. *J. Build. Environ.* **2007**, *42*, 2396–2409. [[CrossRef](#)]

31. Ali-Toudert, F.; Mayer, H. Numerical study on the effects of aspect ratio and solar orientation on outdoor thermal comfort in hot and dry climate. *J. Build. Environ.* **2006**, *41*, 94–108. [[CrossRef](#)]
32. Djenane, M.; Farhi, A.; Benzerzour, M.; Musy, M. Microclimatic behaviour of urban forms in hot dry regions, towards a definition of adapted indicators. In Proceedings of the 25th International Conference on Passive and Low Energy Architecture PLEA, Dublin, Ireland, 25–29 September 2008.
33. Al Jawabra, F.; Nikolopoulou, M. Outdoor Thermal Comfort in the Hot Arid Climate, the effect of socio-economic background and cultural differences. In Proceedings of the 26th Conference on Passive and Low Energy Architecture PLEA 2009, Quebec City, QC, Canada, 22–24 June 2009.
34. Middel, A.; Selover, N.; Hagen, B.; Chhetri, N. Impact of shade on outdoor thermal comfort—A seasonal field study in Tempe, Arizona. *Int. J. Biometeorol.* **2016**, *60*, 1849–1861. [[CrossRef](#)]
35. Lee, I.; Voogt, J.A.; Gillespie, T.J. Analysis and Comparison of Shading Strategies to Increase Human Thermal Comfort in Urban Areas. *Atmosphere* **2018**, *9*, 91. [[CrossRef](#)]
36. Givoni, B. *Climate Considerations in Building and Urban Design*; ITP: New York, NY, USA, 1997.
37. Kakon, A.N.; Nobuo, M. The sky view factor effect on the microclimate of a city environment: A case study of Dhaka city. In Proceedings of the 7th International Conference on Urban Climate, Yokohama, Japan, 29 June–3 July 2009.
38. Lin, T.; Matzarakis, A.; Hwang, R. Shading effect on long-term outdoor thermal comfort. *J. Build. Environ.* **2010**, *45*, 213–221. [[CrossRef](#)]
39. Oke, T.R. Canyon geometry and the nocturnal urban heat island: Comparison of scale model and field observations. *J. Clim.* **1981**, *1*, 237–254. [[CrossRef](#)]
40. Barring, L.; Mattsson, J.O.; Lindqvist, S. Canyon geometry, street temperatures and urban heat island in Malmö, Sweden. *J. Clim.* **1985**, *5*, 433–444. [[CrossRef](#)]
41. Svensson, M.K. Sky view factor analysis implications for urban air temperature differences. *J. Appl. Meteorol.* **2004**, *11*, 201–211. [[CrossRef](#)]
42. Peel, M.C.; Finlayson, B.L.; McMahon, T.A. Updated world map of the Köppen-Geiger climate classification. *Hydrol. Earth Syst. Sci.* **2007**, *11*, 1633–1644. [[CrossRef](#)]
43. ANSI/ASHRAE. *Standard 55: 2017, Thermal Environmental Conditions for Human Occupancy*; ASHRAE: Atlanta, GA, USA, 2017.
44. U.S. Department of Energy. 2012. Available online: http://apps1.eere.energy.gov/buildings/energyplus/cfm/weather_data3.cfm/region=1_africa_wmo_region_1/country=EGY/cname=Egypt (accessed on 16 May 2020).
45. American Society of Heating. *2009 ASHRAE Handbook: Fundamentals*; American Society of Heating: Atlanta, GA, USA, 2009.
46. Toparlar, Y.; Blocken, B.; Maiheu, B.; van Heijst, G.J.F. A review on the CFD analysis of urban microclimate. *Renew. Sustain. Energy Rev.* **2017**, *80*, 1613–1640. [[CrossRef](#)]
47. Amos, K. Envelope Thermal Design Optimization for Urban Residential Buildings in Malawi. *Buildings* **2016**, *6*, 13. [[CrossRef](#)]
48. Sørensen, D.N.; Nielsen, P.V. Quality control of computational fluid dynamics in indoor environments. *Indoor Air* **2003**, *13*, 2–17. [[CrossRef](#)]
49. Blocken, B.; Janssen, W.D.; van Hooff, T. CFD simulation for pedestrian wind comfort and wind safety in urban areas: General decision framework and case study for the Eindhoven University campus. *Environ. Model. Softw.* **2012**, *30*, 15–34. [[CrossRef](#)]
50. Elnabawi, M.H.; Hamza, N.; Dudek, S. Shading Historical Commercial Streets in Hot Arid Areas: Questioning the Common Wisdom. In Proceedings of the 33rd PLEA International Conference: Design to Thrive, PLEA, Edinburgh, UK, 3–5 July 2017; ISBN 9780992895754.
51. Richards, P.J.; Hoxey, R.P. Appropriate boundary conditions for computational wind engineering models using the k- ϵ turbulence model. *J. Wind Eng. Ind. Aerodyn.* **1993**, *46–47*, 145–153. [[CrossRef](#)]
52. Blocken, B.; Stathopoulos, T.; Carmeliet, J. CFD simulation of the atmospheric boundary layer: Wall function problems. *Atmos. Environ.* **2007**, *41*, 238–252. [[CrossRef](#)]
53. Wieringa, J. Updating the Davenport roughness classification. *J. Wind Eng. Ind. Aerodyn.* **1992**, *41*, 357–368. [[CrossRef](#)]
54. Davenport, A.G.; Grimmond, S.B.; Oke, T.R.; Wieringa, J. Estimating the roughness of cities and sheltered country. In Proceedings of the 12th AMS Conference on Applied Climatology, Asheville, NC, USA, 8–11 May 2000.

55. Moonen, P.; Defraeye, T.; Dorer, V.; Blocken, B.; Carmeliet, J. Urban Physics: Effect of the micro-climate on comfort, health and energy demand. *Front. Archit. Res.* **2012**, *1*, 197–228. [CrossRef]
56. Blocken, B.; Gualtieri, C. Ten iterative steps for model development and evaluation applied to Computational Fluid Dynamics for environmental fluid mechanics. *Environ. Model. Softw.* **2012**, *33*, 1–22. [CrossRef]
57. Blocken, B. 50 years of Computational Wind Engineering: Past, present and future. *J. Wind Eng. Ind. Aerodyn.* **2014**, *129*, 69–102. [CrossRef]
58. *Guide for the Verification and Validation of Computational Fluid Dynamics Simulations*; AIAA G-077-1998e; American Institute of Aeronautics and Astronautics: Sunrise Valley Drive, Reston, VA, USA, 1998. [CrossRef]
59. Casey, M.; Wintergerste, T. (Eds.) *ERCOFTAC Best Practice Guidelines: Special Interest Group on Quality and Trust in Industrial CFD*; ERCOFTAC: Bushey, UK, 2000.
60. Blocken, B. Computational Fluid Dynamics for urban physics: Importance, scales, possibilities, limitations and ten tips and tricks towards accurate and reliable simulations. *Build. Environ.* **2015**, *91*, 219–245. [CrossRef]
61. Franke, J.; Hellsten, A.; Schlünzen, H.; Carissimo, B. Best Practice Guideline for the CFD Simulation of Flows in the Urban Environment, Action 732. COST: Brussels. 2007. Available online: http://www.mi.unihamburg.de/fileadmin/files/forschung/techmet/cost/cost_732/pdf/BestPractiseGuideline_1-5-2007-www.pdf (accessed on 20 July 2020).
62. Fanger, P.O. *Thermal Comfort*; McGraw Hill Place City Book: New York, NY, USA, 1972.
63. Nikolopoulou, M.; Steemers, K. Thermal comfort and psychological adaptation as a guide for designing urban spaces. *J. Energy Build.* **2003**, *35*, 95–101. [CrossRef]
64. Dowdy, S.; Wearden, S.; Chilko, D. *Statistics for Research*, 3rd ed.; John Wiley & Sons, Inc.: Hoboken, NJ, USA, 2004.
65. Nakamura, Y.; Oke, T.R. Wind, Temperature and Stability conditions in an East-West Oriented Urban Canyon. *J. Atmos. Environ.* **1998**, *22*, 2691–2700. [CrossRef]
66. Ng, E.; Yuan, C.; Chen, L.; Ren, C.; Fung, J.C.H. Improving the wind environment in high-density cities by understanding urban morphology and surface roughness: A study in Hong Kong. *J. Landsc. Urban Plan.* **2011**, *101*, 59–74. [CrossRef]
67. Ng, E.; Cheng, V.; Chan, C. Urban Climatic Map and Standards for Wind Environment—Feasibility Study. Technical Input Report no. 1: Methodologies and Finds of User’s Wind Comfort Level Survey. Hong Kong Planning Department. 2008. Available online: http://www.pland.gov.hk/pland_en/p_study/prog_s/ucmapweb/ucmap_project/content/reports/Comfort_Level_Survey.pdf (accessed on 1 August 2020).
68. Cheng, V.; Ng, E.; Chan, C.; Givoni, B. Outdoor thermal comfort study in a subtropical climate: A longitudinal study based in Hong Kong. *Int. J. Biometeorol.* **2012**, *56*, 43–56. [CrossRef]
69. Yuan, C.; Ng, E. Building porosity for better urban ventilation in high-density cities—A computational parametric study. *Build. Environ.* **2012**, *50*, 176–189. [CrossRef]
70. Hang, J.; Luo, Z.; Sandberg, M.; Gong, J. Natural ventilation assessment in typical open and semi-open urban environments under various wind directions. *J. Build. Environ.* **2012**, *70*, 318–333. [CrossRef]
71. Asfour, O.; Gadi, M. Using CFD to investigate ventilation characteristics of vaults as wind-inducing devices in buildings. *Appl. Energy* **2008**, *85*, 1126–1140. [CrossRef]
72. Al-Kayiem, H.M.; Firdaus, B.M.; Sidik, M.F.; Munusammy, R.A.L. Study on the Thermal Accumulation and Distribution Inside a Parked Car Cabin. *Am. J. Appl. Sci.* **2010**, *7*, 784–789. [CrossRef]
73. Hadavand, M.; Yaghoubi, M. Thermal behavior of curved roof buildings exposed to solar radiation and wind flow for various orientations. *Appl. Energy* **2008**, *85*, 663–679. [CrossRef]
74. Fathy, H. *Natural Energy and Vernacular Architecture*; University of Chicago Press: Chicago, IL, USA; London, UK, 1986.
75. Wooten, R.D. Statistical analysis of the relationship between wind speed, pressure and temperature. *J. Appl. Sci.* **2011**, *11*, 2712–2722. [CrossRef]
76. Zhang, W.; Hu, W.; Wen, Y. Thermal comfort modeling for smart buildings: A fine-grained deep learning approach. *Ieee Int. Things J.* **2018**, *6*, 2540–2549. [CrossRef]
77. Höppe, P. Heat balance modelling. *Experientia* **1993**, *49*, 741–746. [CrossRef]
78. Hoppe, P. The physiological equivalent temperature—A universal index for the biometeorological assessment. *Int. J. Biometeorol.* **1999**, *43*, 71–75.

79. Matzarakis, A.; Rutz, F.; Mayer, H. Modelling radiation fluxes in simple and complex environments—Application of the RayMan model. *Int. J. Biometeorol.* **2007**, *51*, 323–334. [[CrossRef](#)]
80. Matzarakis, A.; Rutz, F.; Mayer, H. Modelling Radiation fluxes in simple and complex environments—Basics of the RayMan model. *Int. J. Biometeorol.* **2010**, *54*, 131–139. [[CrossRef](#)]
81. Dimiceli, V.E.; Piltz, S.F.; Amburn, S.A. Estimation of Black Globe Temperature for Calculation of the Wet Bulb Globe Temperature Index. In Proceedings of the World Congress on Engineering and Computer Science (WCECS) 2011, San Francisco, CA, USA, 19–21 October 2011.
82. Dimiceli, V.E.; Piltz, S.F.; Amburn, S.A. *Black Globe Temperature Estimate for the WBGT Index*; Springer: Heidelberg, Germany, 2011; pp. 323–334.
83. Hunter, C.H.; Minyard, C.O. Estimating Wet Bulb Globe Temperature Using Standard Meteorological Measurements. In Proceedings of the Conference: 2nd Conference on Environmental Applications, Long Beach, CA, USA, 18 November 1999. WSRC-MS-99-00757.
84. Ohler, L.; Lechleitner, M.; Junker, R.R. Microclimatic effects on alpine plant communities and flower-visitor interactions. *Sci. Rep.* **2020**, *10*, 1366. [[CrossRef](#)] [[PubMed](#)]
85. Duarte, D.H.S.; Shinzato, P.; Gusson, C.D.S.; Alves, C.A. The impact of vegetation on urban microclimate to counterbalance built density in a subtropical changing climate. *Urban Clim.* **2015**, *14*, 224–239. [[CrossRef](#)]
86. Tsoka, S.; Tsikaloudaki, K.; Theodosiou, T.; Bikas, D. Urban Warming and Cities' Microclimates: Investigation Methods and Mitigation Strategies—A Review. *Energies* **2020**, *13*, 1414. [[CrossRef](#)]
87. Taleghani, M. The impact of increasing urban surface albedo on outdoor summer thermal comfort within a university campus. *Urban Clim.* **2018**, *24*, 175–184. [[CrossRef](#)]
88. Gatto, E.; Buccolieri, R.; Aarrevaara, E.; Ippolito, F.; Emmanuel, R.; Perronace, L.; Santiago, J.L. Impact of Urban Vegetation on Outdoor Thermal Comfort: Comparison between a Mediterranean City (Lecce, Italy) and a Northern European City (Lahti, Finland). *Forests* **2020**, *11*, 228. [[CrossRef](#)]
89. ISO 7730. Ergonomics of the Thermal Environment. In *Analytical Determination and Interpretation of Thermal Comfort using Calculation of the PMV and PPD Indices and Local Thermal Comfort Criteria*; ISO: Geneva, Switzerland, 2005.
90. Lin, T.-P. Thermal perception, adaptation and attendance in a public square in hot and humid regions. *Build. Environ.* **2009**, *44*, 2017–2026. [[CrossRef](#)]

Publisher's Note: MDPI stays neutral with regard to jurisdictional claims in published maps and institutional affiliations.



© 2020 by the authors. Licensee MDPI, Basel, Switzerland. This article is an open access article distributed under the terms and conditions of the Creative Commons Attribution (CC BY) license (<http://creativecommons.org/licenses/by/4.0/>).